Title
Tailoring Surface Opening of Hollow Nanocubes and Their Application as Nanocargo Carriers

Journal
ACS Central Science, 4(12)

ISSN
2374-7943

Authors
Lu, Fang
Xin, Huolin
Xia, Weiwei
et al.

Publication Date
2018-12-26

DOI
10.1021/acscentsci.8b00778

ACS central science

Research Article

Cite This: ACS Cent. Sci. 2018, 4, 1742−1750

http://pubs.acs.org/journal/acscii

Tailoring Surface Opening of Hollow Nanocubes and Their Application as Nanocargo Carriers

Fang Lu,*[,†,▽] Huolin Xin,[†,▽,○] Weiwei Xia,[†] Mingzhao Liu,[†] Yugang Zhang,[‡] Weiping Cai,[§,∥] and Oleg Gang[†,⊥,#]

[†]Center for Functional Nanomaterials, Energy & Photon Sciences Directorate, Brookhaven National Laboratory, Upton, New York 11973, United States

[‡]National Synchrotron Light Source II, Energy & Photon Sciences Directorate, Brookhaven National Laboratory, Upton, New York 11973, United States

[§]Key Lab of Materials Physics, Anhui Key Lab of Nanomaterials and Nanotechnology, Institute of Solid State Physics, Chinese Academy of Sciences, Hefei 230031, P. R. China

[∥]Department of Materials Science and Engineering, University of Science and Technology of China, Hefei 230026, P. R. China

[⊥]Department of Chemical Engineering, Columbia University, New York, New York 10027, United States

[#]Department of Applied Physics and Applied Mathematics, Columbia University, New York, New York 10027, United States

Supporting Information

ABSTRACT: Hollow nanoparticles (NPs) are of broad interest for biomedical, optical, and catalytic applications due to their unique geometry-related physicochemical properties. The ability to engineer hollow structures with surface openings is particularly attractive since emergent properties are promised by the design of shell porosity and encapsulation of guest materials. However, it still remains challenging to precisely control the opening of the hollow structure, in terms of shape, size, and location. Here, we report a facile *one-step* strategy to synthesize a hollow nanostructure with well-defined cubic-shape openings at the corners, by regulating nanoscale galvanic replacement processes with specific surface-capping agents. The final product is a single-crystalline AuAg alloy which morphologically features three "belts" orthogonally wrapping around a virtual cube, denoted by *nanowrapper*. We demonstrate a structural tunability of our synthetic method for tailoring nanowrapper and the corresponding tuning of its plasmonic band from the visible to near-infrared (NIR) range. Advanced electron tomography techniques provide unambiguous three-dimensional (3D) visualizations to reveal an unconventional transformation pathway of sharp-cornered Ag nanocube to nanowrapper and correlate its structure with measured and computed spectroscopic properties. Importantly, we find that the surfactant, i.e., cetylpyridinium chloride (CPC), is crucial for the openings to be localized at the corners of the hollow cube and be tailored to a cubic shape in our one-step process. Furthermore, such a well-defined hollow architecture also allows a guest nano-object to be contained within, while the large openings at corners enable controlled loading/release of nanoscale cargo, a DNA-coated particle, using change of ionic conditions. This work expands our understanding of surface engineering in nanoscale galvanic replacement reactions and opens new ways toward the shape control of hollow NPs.

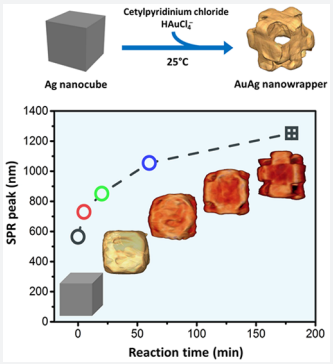

INTRODUCTION

Hollow metal nanostructures have attracted extensive attention in the past few decades due to their unique physicochemical properties, often deviating sharply from their solid counterparts.[1] They have shown promise for a variety of applications, including catalysis,[2] optical sensing,[3] and biomedicine.[4] Many morphologies of hollow metal nanostructures have been investigated, including nanoboxes,[5] nanoshells,[6] nanocages,[7] and nanoframes.[8,9] The large interior void in hollow nanostructures yields an enhanced surface-to-volume ratio.[10,11] That allows tuning significantly plasmonic characteristics of the nanoparticle (NP) from the visible to near-infrared (NIR) range.[12] More interestingly, the ability of introducing surface pores to hollow structures allows for loading and encapsulating foreign materials, including drugs, biological molecules,[4,13] and, potentially, nanoparticles (NPs), for engendering new functionalities. For instance, distinct from nanoshells and nanoboxes with inaccessible interiors, hollow architectures featuring surface pores, e.g., nanocage, are capable of loading molecular-scale materials into the inner void via accessible channels, which is promising for nanoparticle, gene, and drug delivery.[4] However, engineering the surface opening with precise size, shape, and location is challenging. Particularly, an outstanding challenge is to generate hollow structures with large pores that permit the loading and encapsulation of guest NPs. Such an attractive yolk−shell motif would enable tailored fabrication of nano-

Received: October 25, 2018
Published: December 12, 2018

DOI: 10.1021/acscentsci.8b00778
ACS Cent. Sci. 2018, 4, 1742−1750

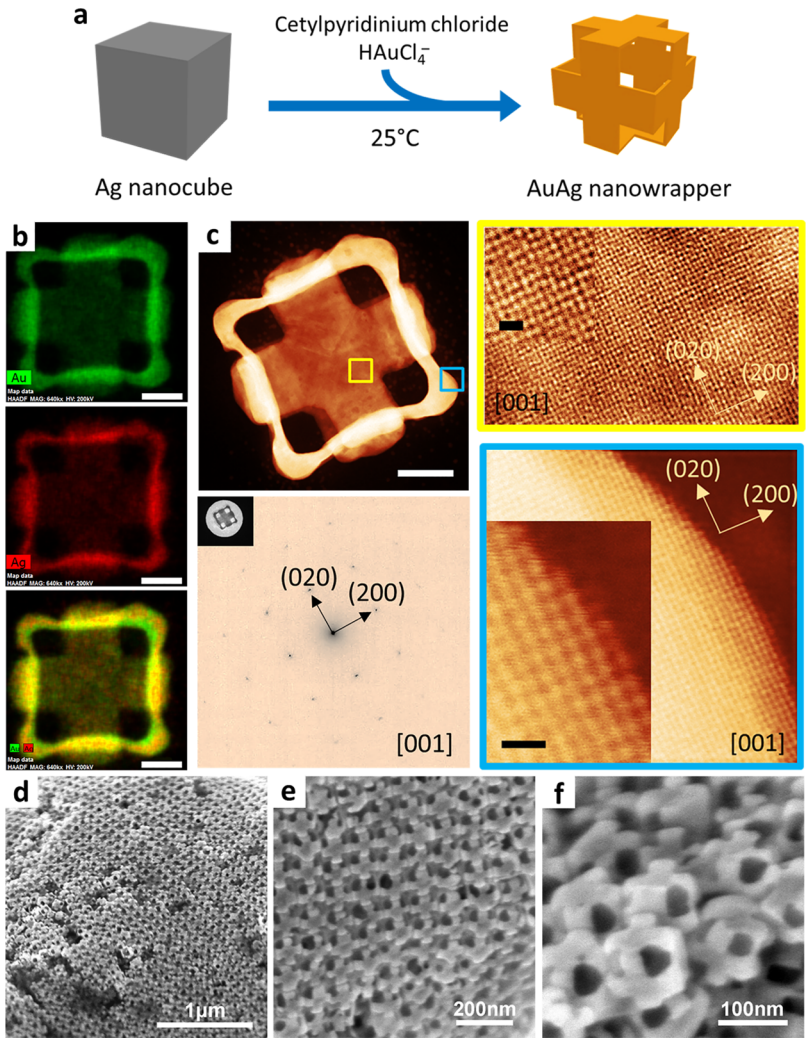

Figure 1. Synthesis of AuAg alloy nanowrappers and the morphological and structural characterizations. (a) Schematic illustration of the one-step synthesis of AuAg nanowrapper using Ag nanocube as sacrificial template. (b) HAADF-STEM characterization and EDX elemental mapping of a single AuAg alloy nanowrapper obtained after 3 h of reaction (Au, green; Ag, red; scale bars are 30 nm). (c) HAADF-STEM image (scale bar is 30 nm), electron diffraction pattern along a [001] zone axis direction, and high-resolution TEM (HRTEM) images of local areas marked by different color frames (scale bars are 0.5 nm). (d) Typical large-area, (e) locally magnified, and (f) high-magnification SEM images of the as-prepared AuAg nanowrappers obtained after 3 h of reaction.

composites exhibiting emergent properties that depend on the intimate colocation of the two nanoscale species.[14,15] For instance, appropriate choice of materials for the encapsulator and encapsulant could be used for catalytic nanoreactors which are optimized for particular small-molecule chemistry, or for derivatization of the encapsulated nanoparticle. The electromagnetic field within integrated complex nanostructures could be tailored to offer significant enhancement for sensitive detection of analytes.[16] However, in general for yolk−shell nanostructures, a core particle in the hollow shell cannot be rationally changed once encapsulated.[17,18] If the encapsulation can be reversibly controlled, then hollow nanoarchitectures could be used for loading, transport, and release of nanoscale cargo, and for the creation of novel stimulus-responsive[19,20] and reconfigurable materials.[21,22]

Current synthetic strategies have allowed introducing small pores to the shells of hollow nanostructures.[15] Those small pores are limited to molecular-scale loading, but not *nanoscale* objects. For example, porous Au nanocages have been synthesized via galvanic replacement involving $HAuCl_4$ and Ag nanocubes with sharp corners.[23] However, the pores of such nanocages are small, polydisperse in size/shape, and randomly distributed across the surfaces. These materials are only suitable to carry molecular-scale species.[13,24] It is nontrivial to directly enlarge the pores on the faces of nanocages because an over-reaction could lead to the formation of nanoframes,[25] which are too open to hold guest objects within the interior,[2] or even can collapse.[23] In addition to a rational control of pore size, localizing an opening of pores at the corners of the cube allows enlarging of pores without compromising structural integrity. Much effort has been focused on multistep processes to control the opening location of pores. These processes usually involve a pretreatment of sacrificial templates, i.e., Ag nanocubes, to obtain suitable shape or chemical composition for the subsequent hollowing reactions. For instance, Chen et al. pretreated the Ag nanocubes to have their corners truncated via a thermal annealing process and then used them as templates to obtain AuAg nanocages with pores confined to the corners.[7] Sun et al. synthesized cubic nanocages with openings at the corners

DOI: 10.1021/acscentsci.8b00778
ACS Cent. Sci. 2018, 4, 1742−1750

through a four-step procedure, which includes selectively depositing Ag_2O at the corners of Ag nanocubes in advance, the conformal deposition of Au on the side faces, selectively removing the corner Ag_2O patches, and etching away the Ag core with H_2O_2.[26] However, these corner pores have been limited to being 10 nm in size and triangular in shape, and most importantly, a majority of the obtained nanocages still exhibited unperforated shells. Further enlargement of triangular pores resulted in a split of these structures into separate fragments. Thus, it remains challenging to synthesize nanoarchitectures that are hollow and precisely engineered as porous with high yield and high fidelity of openings via a one-step process.

It is well-known that molecular surfactants can change the surface energy of metal NPs through preferential capping to direct the metal atom deposition on specific crystalline facets and affect the growth kinetics, commonly used in solution-based syntheses to control the shape of particles.[27−29] However, the effect of surfactants on the shape transformation of NPs in a *reverse* growth reaction, i.e., a galvanic replacement converting solid NPs to hollow structures, still remains poorly understood.

Here, we demonstrate a new strategy for engineering a chemical pathway to tailor the pore opening of hollow NPs, in aspects of their size, shape, and location, by regulating nanoscale galvanic replacement processes with specific surface-capping agents. We develop a simple one-step procedure to synthesize a type of AuAg hollow nanostructure—namely, *nanowrapper*—which consists of three "belts" orthogonally wrapping around a cube-shaped void. The nanowrapper features large cubic-like pores at the corners and a cross-belt framework. They are prepared by using sharp-corner Ag nanocubes as the sacrificial templates and cetylpyridinium chloride (CPC) as the surfactant in galvanic replacement between $HAuCl_4$ and Ag at room temperature. Viewed along the normal direction of one cross-belt side face, the pores are square in shape and up to 31 ± 3 nm in edge length. Electron tomography was used for three-dimensional (3D) visualization of the morphological and chemical architecture of the nanoparticles during the evolution from sharp-corner cube to wrapper. Significant differences with respect to the reported conventional nanoscale galvanic replacements were observed: with the assistance of CPC, even starting from sharp-corner Ag cubes, surface openings can be localized at the corners of the hollow cube and further tailored to be large and cubic in a one-step process. Spectroscopic measurements allowed correlating the dependence of the plasmonic signature with the degree of corner opening. Nanowrapper with large open corners shows promise as a carrier of functional NPs, due to the size compatibility between pore and encapsulation spaces. We demonstrate that, by taking advantages of the ionic-strength-dependent configuration of DNA chains, the large openings at the corners of nanowrappers can be used for loading and releasing NPs in a controllable manner.

DISCUSSION

Figure 1A schematically illustrates a one-step process employed in the synthesis of AuAg nanowrappers. In a typical process, the Ag nanocubes are dispersed in an aqueous CPC solution, followed by injecting aqueous $HAuCl_4$ under magnetic stirring at room temperature. The reaction continues for 3 h and is quenched by centrifugation (Materials and Methods section in the Supporting Information). We used Ag nanocubes[30,31] as the sacrificial templates. These single-crystalline nanocubes with sharp corners are uniform with an average edge length of ∼100 nm (Figure S1). The galvanic replacement reaction occurred once the nanocubes dispersed in CPC were mixed with aqueous $HAuCl_4$.

Transmission electron microscopy (TEM) observations reveal that the measured projected contours of NPs after 3 h of galvanic replacement reaction exhibit a square frame with a belt-made cross on the center of each face, and four square holes at the corners (Figure S2). Figure 1b shows a high-angle annular dark-field scanning transmission electron microscopy (HAADF-STEM) image and energy-dispersive X-ray (EDX) spectroscopy elemental mapping of 3 h old products. As shown in Figure 1 and Figure S2, the frames are ∼112 nm in edge length, with a wall thickness of ∼8 nm on average, but with a measurable thickening to ∼15 nm near bends (edges of the original cube). The centered cross-belt is intact and smooth, each branch of which has a width of ∼38 nm. STEM and the corresponding quantitative EDX mapping images in Figure 1b demonstrate that the particles are hollow and composed of AuAg alloy (66% Au and 34% Ag). High-resolution (HR) HAADF-STEM analysis shows that they are single crystals with the AuAg face-centered cubic (fcc) structure (Figure 1c). The bends of the encircling "belts" exhibit high-index crystallographic planes due to their high curvature. As a result of the high uniformity of products, the formed particles self-assemble into ordered and well-packed superlattices over large areas, which appear as a network with squared porous patterns, as observed from the low-magnification SEM image (Figure 1d,e). The particles are hollow, as confirmed by the tilt view through isolated particles (Figure 1f).

To characterize the 3D morphology and chemical composition, we conducted HAADF-STEM and STEM-EDX electron tomography. A tilt series of HAADF-STEM and EDX projection images were acquired and used as an input of 3D reconstruction. The result of this process reveals that the obtained NPs are thin-walled hollow cubes with square holes at the four corners of every {100} facet, which displays a cross-shaped wall viewed along the [100] direction (Figure 2a,b, Movie S1, and Figure S3). We refer to this architecture as a nanowrapper since it can be thought of as three long two-dimensional belts orthogonally wrapping around a cube-shaped inner void (Figure $2a_3$, $2b_3$). The nanowrapper is flexible due to its lack of central support as well as the thin shell. We observed a slight deformation under a tomographic electron beam exposure (Figure $2a_1$,b_1), while no such effect was visible under conventional SEM conditions (Figure 1d−f). The 3D-EDX tomography provides a visualization of the chemical architecture of the particles. The results confirmed the formation of Au/Ag alloy shell with nearly uniform element distribution, which has a composition ratio of 66:34 (Figure $2a_1$,b_1). The optical extinction spectrum of the nanowrappers features a strong mode at ∼1250 nm and a much weaker mode at ∼590 nm (Figure 2c). Using the frequency domain finite element method (FEM) (Supporting Information, Figure S4) and nanowrapper dimensions measured from TEM, we numerically simulated the extinction spectrum and reproduced both modes in high fidelity (Figure 2c,d). Analysis of the near-field and far-field patterns indicates that both modes correspond to plasmon oscillations parallel to the nanowrapper outer facets. However, the lower energy mode (P1 at 1250 nm) is purely dipolar (radiant), while the higher energy mode (P2 at 590 nm) mixes dipolar and

DOI: 10.1021/acscentsci.8b00778
ACS Cent. Sci. 2018, 4, 1742−1750

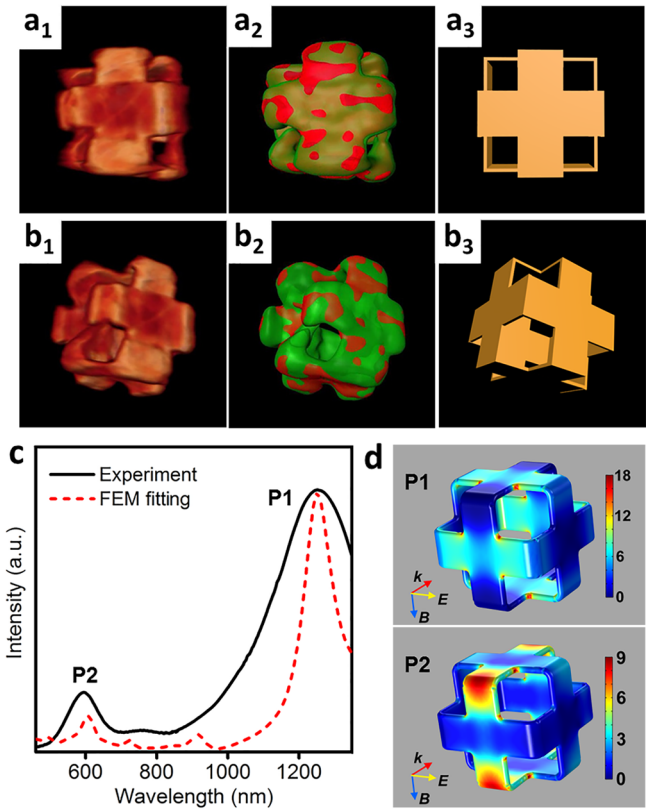

Figure 2. Three-dimensional morphology, chemical composition, and structure-correlated optical characterizations for a single AuAg alloy nanowrapper obtained after 3 h of reaction. (a, b) From left to right (subscript: 1−3), 3D tomography rendering, the corresponding 3D EDX rendering, and 3D model images of a AuAg alloy nanowrapper viewed along (a) [001] and (b) tilted directions (Au is green, and Ag is red in a_2 and b_3). (c) Optical extinction spectrum of the nanowrappers: experimental (black solid line) and numerically simulated (red dash line) by the frequency domain finite element method (FEM). (d) The gray-background profiles (P1 and P2) are calculated by electric field enhancement $P = |\vec{E}|^2/|\overrightarrow{E_0}|^2$ at the AuAg nanowrapper surface for the respective resonance modes, corresponding to surface plasmonic resonance (SPR) peaks shown in optical extinction spectra.

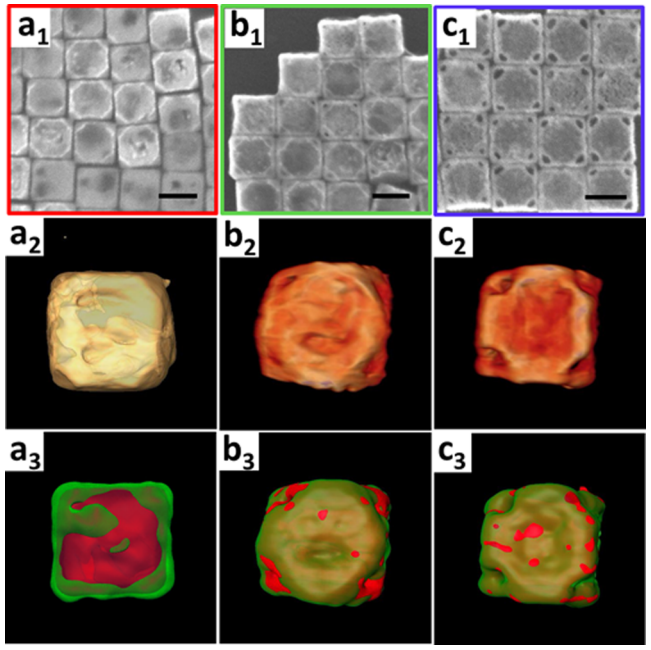

Figure 3. Morphology and chemical composition characterizations of the products obtained at different intermediate stages during the transformation of Ag nanocubes into AuAg nanowrappers. From left to right (subscript: 1−3): SEM, reconstructed 3D volume rendering, and the corresponding 3D EDX rendering images of nanoparticles obtained after different reaction times (a, 5 min; b, 20 min; c, 60 min). Scale bars for the SEM images are 100 nm. In EDX images of a_3, b_3, and c_3, Au and Ag are green and red, respectively.

quadrupolar (subradiant) features (Figure 2d). Numerical calculation suggests that the resonant energy of the dipolar mode is highly sensitive to the nanowrapper thickness. The subradiant character is responsible for the low spectral strength of the 590 nm mode. Distinct presentation of the high energy mode at 590 nm is attributed to the morphology features from the good "bending" of uniform belts at edges.

To investigate the mechanism responsible for the formation of AuAg nanowrappers, we carried out complementary analyses via characterization of time-dependent morphological evolution during reaction, by means of SEM, 3D-HAADF-STEM tomography, and 3D-STEM-EDX tomography (Figure 3a−c). In a typical galvanic replacement reaction, $AuCl_4^-$ generates one Au(0) atom at the expense of every three Ag(0) atoms. We observed that, as Ag nanocubes reacted with the $HAuCl_4$ solution at an early stage (1 min), pitting took place on the side faces of the Ag nanocube, through which the oxidized Ag^+ ions leach out. Meanwhile, the corners of nanocubes became slightly truncated at this point because of the oxidation of Ag (Figure S5). We observed that the truncation of the cube corners happened simultaneously with the formation of pinholes on {100} facets. This is radically different to what has been reported previously for galvanic replacement in Ag nanocubes, both with and without sharp corners.[7,23] As the reaction proceeded further (5 min), the pinholes on {100} facets became larger, which continued to serve as the exclusive channels for the released electrons inside the Ag cube to easily migrate out (Figure 3a_1). The truncation-induced triangle {111} facets on the corner site became pronounced.

Tomography reconstructions of the product at this stage demonstrate the partial hollowing of the cube (Figure 3a_2). A thin layer of Au was deposited on the surface of the cuboid (Figure 3a_3). As the reaction proceeded to 20 min, the inner void visibly grew (Figure 3b_1). Pores began to open on the truncation-induced triangle {111} facets, while the pinhole on the side faces tended to shrink (Figure 3b_1,b_2). The surface was enriched with Au except around the corner-localized pores (Figure 3b_3). Upon a continuation of the reaction to 1 h, the void inside the cube increased. The corner pores became larger, whereas the pores on the side faces disappeared (Figure 3c_1,c_2). More Ag was detected on the exterior surface than that at the 20 min reaction stage because of the alloying process; the homogeneous AuAg alloy is more stable than either pure Au or Ag (Figure 3c_3). A subsequent dealloying stage allows Ag to be removed from the alloyed walls. The resultant lattice vacancies were released through surface reconstruction that makes the corner pores larger and square-shaped. After 3 h of reaction time, the nanowrapper architecture was fully formed, including thin walls and smooth surfaces (Figure 1). The cubic pores only appeared at the corners, so the cross-belt wall was on each {100} face.

DOI: 10.1021/acscentsci.8b00778
ACS Cent. Sci. 2018, 4, 1742−1750

The morphological and compositional evolution of NPs leads to corresponding changes in extinction spectra (Figure 4a). The dipolar surface plasmonic resonance (SPR) band red-shifts from 565 to 1250 nm, along with a structural transformation of cubes to nanowrappers (Figure 4b). Initially, the Ag nanocubes exhibited a broad dipole peak at 565 nm, together with three shoulder peaks at 347, 394, and 471 nm. Three shoulder peaks correspond to higher-order plasmonic modes. Their separated and distinct profiles indicate the structural features of Ag nanocubes with sharp corners and edges.[32] After the reaction continued only for 5 min, an obvious intensity decrease for the SPR peaks of silver was observed, especially for the three shoulder peaks at shorter wavelengths, while the extinction peak at longer wavelength red-shifted to 730 nm. This spectral change can be attributed to the deposition of a thin gold layer on the surfaces of Ag templates, accompanied by the truncation and partial hollowing of the Ag cube. The silver LSPR peaks almost disappeared after 20 min of reaction, and the extinction peaks at long wavelength red-shifted to 851 nm. This spectral change could be related to the increase in void size and the reduction in wall thickness of truncated boxes with small corner openings. After the reaction continued for 1 h, the extinction peak was further red-shifted to 1055 nm, as a result of the size increase of corner pores as well as the further reduction of wall thickness during the alloying and dealloying process. Finally, at 3 h, the extinction peak red-shifted to 1250 nm, and a new peak appeared at 590 nm; that corresponds to our structural observation of the formation of nanowrappers with smooth surfaces and large corner openings. A series of cubic hollow nanostructures with tunable corner-opening size and wall thickness exhibit strong absorption in the near-infrared region (800−1200 nm), endowing them with potential value in biomedical applications such as photothermal therapy, photo-induced drug delivery, and contrast-enhanced imaging.

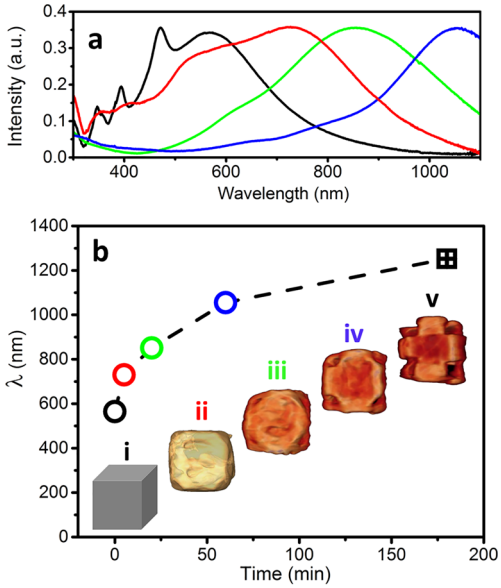

Figure 4. The morphological evolution of NPs leads to corresponding changes in extinction spectra. (a) UV−vis−NIR extinction spectra of Ag nanocubes after the galvanic replacement reaction proceeded for 0 min (black), 5 min (red), 20 min (green), and 60 min (blue). (b) Plot showing that the dipolar surface plasmonic resonance (SPR) peak, P1, of products red-shifts with increase in the reaction time. Inset shows a summarized transformation pathway where Ag nanocubes are reacted with $AuCl_4^-$ to form AuAg alloy nanowrappers (i, 0 min; ii, 5 min; iii, 20 min; iv, 60 min; v, 180 min). The color of circles (i−iv) in the plot is consistent with that of curves in Figure 4a, except that at 180 min (v) corresponding to the curve in Figure 2c.

Previous studies have attributed the formation of a hollow, porous AuAg nanocage to the mechanism commonly referred to as "nanoscale galvanic replacement" between $HAuCl_4^-$ and well-formed Ag particles.[33] For the case of the cubic nanocage (Figure 5a), the reaction pathway mainly involves pitting at the surface of sharp-corner cube to hollow-out Ag (pinhole formation), central void formation (nanobox), alloying and dealloying of shell (sieve), and pore generation in the shell due to the coalescence of lattice vacancies (nanocage).[23] However, in the reported one-step synthesis processes, pores formed in the shell are usually randomly distributed around the surface of nanocage. On the other hand, using Ag nanocubes with truncated corners as sacrificial templates has been demonstrated to enable assigning corners as primary sites for pore opening.[7] Previously, for the confinement of the pore opening at the corners of nanocages in the reported studies, an extra step prior to the conventional synthesis of nanocages has to be taken to truncate the corners of cubes to obtain qualified sacrificial templates.[9]

Here, we propose a new strategy to utilize the preferential surface-capping properties of surfactants to precisely engineer the pores on the surface of nanocages in a *one-step* synthesis process, in aspect of size, shape, and location. In particular, we aim to only open the pores at the eight corners of the hollow cube. We select CPC as surfactant to allow both corner truncation and hollowing-out reactions to happen simultaneously. According to our previous studies,[32] since CPC preferentially caps the {100} rather than {111} facets of Ag, it is commonly used in the seed-mediated synthesis of Ag nanocubes with sharp-corners.[34] As shown in the present results (Figure 5b), at the early stages, the pinholes form on Ag {100} facets and serve as the primary site to hollow-out the Ag cube, which is same as the conventional process. However, because of the week absorption of CPC on Ag cube sharp corners, the cubes are truncated by oxidative etching of Ag, leading to exposing the {111} facets of Ag. As the galvanic replacement reaction between $HAuCl_4^-$ and fresh and active Ag atoms proceeds at the exposed {111} facets, the pores open and become large gradually on the {111} facets while the pinholes on the {100} facets disappear with the hollow center void forming at a certain stage. In the following alloying and dealloying process, the vacancy-induced porosity appears on the {100} side facets of AuAg alloy. Subsequently, with assistance of CPC, the in-wall vacancies coalesce into big square holes at the corners through a surface rearrangement process to efficiently release lattice vacancies. The specific shape of square pores could be related to the square arrangement of atoms on each wall where the surface is mainly bound by {100} crystallographic planes.

The shape evolution mechanism in our system is also quite different from the reported two-step nanocage method.[7] First, in the latter, sharp corners of Ag cubes are truncated via a thermal annealing process in advance. Second, by using pretruncated Ag cubes as sacrificial template, while there is no opening on the side faces, the corner area is assigned as exclusive sites for the hollowing-out of the Ag cube and eventually becomes triangular pores at eight corners of a nanocage. The obtained products with the Au content of <60%

DOI: 10.1021/acscentsci.8b00778
ACS Cent. Sci. 2018, 4, 1742−1750

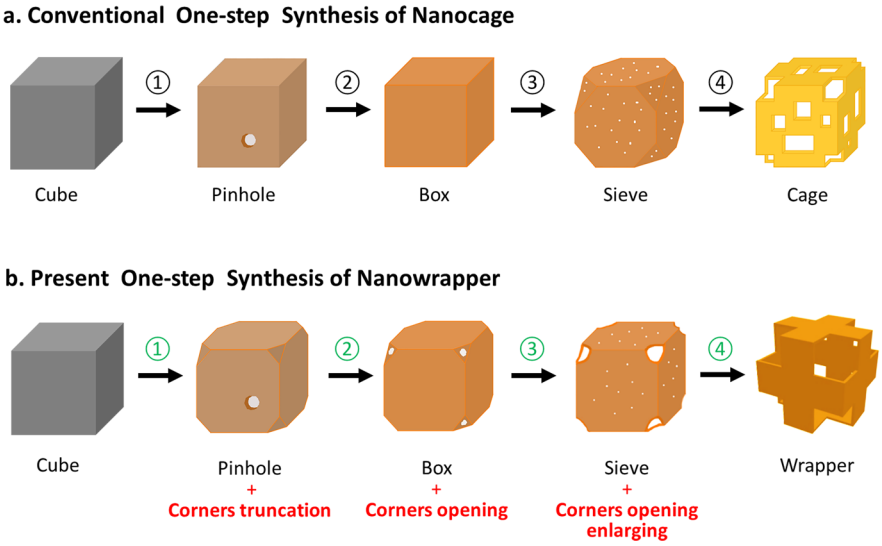

Figure 5. Comparison of transformation pathway between one-step syntheses of nanocage and nanowrapper using sharp-corner Ag cubes as sacrificial templates. (a) For the case of the cubic nanocage, the conventional reaction pathway mainly involves (1) pitting on the {100} surface of the cube to hollow-out Ag (pinhole), (2) formation of the central void with a seamless Au−Ag alloy shell (box), (3) dealloying process to reconstruct the shell and generate small pinholes (sieve), and (4) pore generation in the shell due to the coalescence of lattice vacancies (nanocage with pores randomly distributed on the surface). (b) For the case of the nanowrapper, the reaction pathway mainly involves (1) pitting on the {100} surface of the cube to hollow-out Ag while truncating the cube corners (pinhole + corners truncation), (2) formation of a central void with a Au−Ag alloy shell while small openings appear at the truncated corner (box + corner openings), (3) dealloying process to generate small pinholes while the corner openings become large gradually (sieve + corner openings enlarging), and (4) formation of big square pores at the corners due to the coalescence of lattice vacancies with the assistance of CPC (nanowrapper with large cubic pores at all corners).

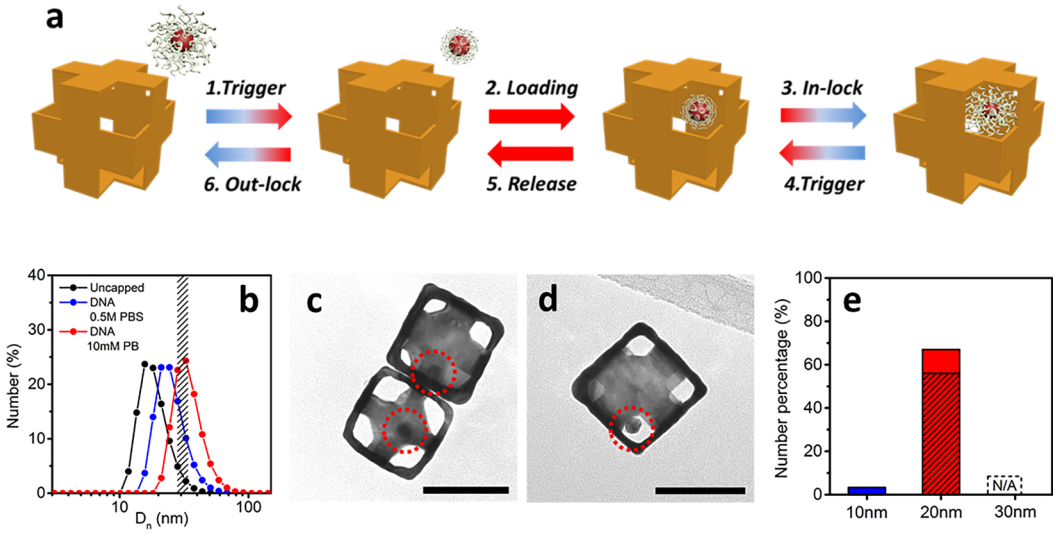

Figure 6. Nanowrapper-based carrier for nanoscale cargo. (a) Schematic for using nanowrapper as a carrier to load and release a DNA-capped nanosphere. Blue and red shades on direction arrow bars mean low (e.g., 10 mM phosphate buffer) and high (e.g., 0.5 M PBS) ionic strength, respectively. (b) Dynamic light scattering (DLS) results for the isolated uncapped Au SNPs, DNA-capped Au SNPs in 0.5 M PBS, and DNA-capped Au SNPs in 10 mM phosphate buffer, respectively, and a comparison with the size of the at-corner pores of nanowrappers (black-dashed-line-marked area). (c, d) Typical TEM images of nanowrappers with the DNA-capped 20 nm Au NPs encapsulated. Scale bars for the TEM images are 100 nm. (e) A population histogram for the proportion of nanowrappers with nanoparticles encapsulated as a function of nanoparticles size is obtained based on the analysis of about 200 nanowrappers (in the red column, the black-dashed-line-marked and unmarked areas correspond to the proportions of nanowrappers with one NP and two NPs inside, respectively).

have been demonstrated as a result of the galvanic replacement reaction (Figure S6).

In our one-step approach, the large pores located at all corners of the nanobox show distinct *square-like* shapes, making the final shape as three belts orthogonally wrapping around a virtual cube, and the final products are so-called "nanowrappers". Additionally, the nanowrappers with a relatively high ratio of Au are the results of the reaction wherein the pinholes on the {100} facets are primary sites for hollowing-out of Ag; thus, not only the galvanic replacement reaction but also the dealloying and vacancy-coalescent processes are involved.

We further investigated the roles of surfactant in the present one-step strategy. Interestingly, we find that truncation of cube

DOI: 10.1021/acscentsci.8b00778
ACS Cent. Sci. 2018, 4, 1742−1750

corners is not sufficient for achieving the unique exotic structure of the nanowrapper. It is well-known that CTAB also preferentially absorbs on the Ag {100} facets. Thus, we used cetyltrimethylammonium bromide (CTAB) instead of CPC, to perform a control experiment (Figure S7). As expected, we observed a corner truncation at the initial stage. However, the openings have not formed on the truncated area at all. Pores were rather randomly distributed on the {100} side faces in the final products, similar to the conventional nanocage. This non-pore-opening corner could be understood because the exchange reaction on the truncated area is being highly suppressed because of the stronger protection of CTAB on Ag {111} than that of CPC.[35] Additionally, the usage of CPC and CTAB leads to forming completely different hollow nanostructures. It also indicates that the high-concentrated surfactants in the reaction solution, rather than the residuals of original surfactant (PVP) on the Ag surface, play a dominate role in regulating nanoscale galvanic replacement processes.

Our experiments reveal that reaction temperature plays an important role in the formation of nanowrappers. When the temperature was reduced from 25 to 18 °C, Ag nanocubes were transformed into cubic hollow nanostructures with many pores distributed over the surface. These pores were irregular in size and shape, making the walls fragile and leading to collapse of the nano-objects (Figure S8). This observation suggest that the galvanic replacement and alloying−dealloying processes is strongly temperature-dependent. As the temperature decreases, the rate of atom diffusion and rearrangement, which are responsible for morphological reconstruction, decreases, leading to coarsening and imperfections.

The high-quality nanowrappers obtained with optimized synthetic conditions feature hollow interiors and large openings at all the corners, which allows their use as a new type of carrier for nanoparticles, with controllable loading and release. Figure 6a shows a schematic of the nanowrapper-based system for carrying a nanoparticle whose responsive shell allows for modulating a particle size. DNA is used as a stimulus-responsive component grafted to the particle's surface, and its conformational change can be manipulated by ionic strength in solution.[32,36,37] We use spherical the Au NP (SNP) as a model cargo in the current experiment. Initially, the nanowrapper and Au SNP are separated in the solution of a low ionic strength (e.g., in 10 mM, phosphate buffer), and the SNP diameter is larger than the size of the corner opening. Triggered by increasing ionic strength (e.g., in 0.5 M phosphate buffer saline, PBS), DNA chains shrink because of charge screening, which causes a reduction in the effective size of SNPs with soft DNA shells (step 1).[36] As the SNP diameter becomes small enough to penetrate a nanowrapper through corner pores, loading can occur (step 2). Then, the ionic strength is decreased (e.g., 10 mM phosphate buffer), whereupon the surface-bound DNA shell responsively switches to a stretched conformation due to the electrostatic repulsion between DNA chains. The larger effective size of the SNP thereby confines it within the nanowrapper in a step of in-lock (step 3). The release and out-lock of SNPs can be achieved through a reverse process of increasing and then decreasing the ionic strength (steps 4−6 in Figure 6a).

In the present study, we used Au SNP (~20 nm in diameter) capped with 30-base single-stranded (ss) DNA to demonstrate the realization of this idea. Dynamic light scattering (DLS) results show that isolated uncapped Au SNPs, DNA-capped Au SNPs in 0.5 M PBS, and DNA-capped Au SNPs in 10 mM phosphate buffer have hydrodynamic diameter values (D_h) of ~18.3, ~25.6, and 34.7 nm, respectively (Figure 6b). These values correspond to a DNA-capping thickness (T) of ~3.7 and 8.2 nm for DNA-capped Au SNPs in 0.5 M PBS and 10 mM phosphate buffer, which reveals the conformational changes of DNA depending on the ionic strength in solution.[38] The results show that, compared to the size of pores of the nanowrapper (~31 nm), the effective size of SNPs becomes smaller than a corner opening in 0.5 M PBS (~25.6 nm), and then, in 10 mM phosphate buffer, it becomes larger (~34.7 nm). This ionic-strength-dependent size change enables 20 nm SNP transporting through the pores at the high ionic strength and being encapsulated inside the nanowrapper at the low ionic strength. Figure 6c,d shows typical TEM images of nanowrappers with the DNA-capped 20 nm Au SNPs encapsulated, which are obtained after the step of in-lock (Figure S9). A large fraction of nanowrappers (~67%) were observed having the 20 nm SNPs carried inside, as shown by the population analysis based on the TEM characterization of about 200 nanowrappers (Figure 6e).

The 20 nm Au SNPs have an absorption peak at 528 nm that adjoins the one of the nanowrapper at 590 nm. However, we found that having 20 nm Au SNPs locked inside the nanowrappers brings little change to the UV−vis spectrum of nanowrappers, which also agrees with our numerical simulation based on the frequency domain finite element method (Figure S10). It is attributed to the fact that the extinction cross-section of the nanowrapper is ~80 times larger than that of the 20 nm Au SNP. Therefore, to confirm the loading of 20 nm Au SNPs into the nanowrappers after the in-lock process by optical spectroscopy, we measured the UV−vis spectrum of the supernatants after Au SNPs were released, and the nanowrappers self-precipitated completely. After being obtained through the in-lock step, the loaded nanowrappers with SNP inside were kept undisturbed in the 10 mM phosphate buffer for 6 h, and they settled down naturally under gravity because of their large size. No UV−vis intensity at 528 nm was detected from the supernatant, which confirms that the Au SNPs remained inside of nanowrappers. However, after the ionic strength of the sample solution increased, followed by the self-sedimentation of nanowrappers, a signal at 528 nm from the UV−vis spectrum of the supernatant was observed, indicating a release of 20 nm Au SNPs from the nanowrappers.

The size of DNA-capped SNPs has a dramatic effect on their loading efficiency into nanowrappers. We performed control experiments by using 10 and 30 nm SNPs, both of which are functionalized with the same 30ss DNA (Figure 6e). It is found that 10 nm SNPs coated with DNA are hardly locked inside the nanowrappers because of their small size, where even the conformal expanding of the DNA layer in 10 mM phosphate does not affect their transport through a pore. Meanwhile, 30 nm SNPs cannot be loaded inside the nanowrappers since their effective size with DNA corona is larger than the pores even at the high ionic strength (Figure S11 and Table S1). For both cases, the UV−vis spectra of supernatant measured after the releasing and out-lock steps show no SPR signal from Au SNPs. It confirms that the too small or too large SNPs are not suitable for nanowrappers to carry. Taken together, these results demonstrate a control of loading and a size-selective release of nanocargo within the nanowrappers through the selection of an appropriate DNA-capped shell and core particle size and by switching the shell state.

DOI: 10.1021/acscentsci.8b00778
ACS Cent. Sci. 2018, 4, 1742−1750

CONCLUSION

In summary, we have demonstrated a facile one-step method to synthesize Au−Ag alloy nanowrapper with well-engineered pore opening via room-temperature galvanic replacement. The 3D tomography analysis of the products obtained at different reaction stages reveals an unconventional mechanistic path from the Ag cubes with sharp corners to the nanowrappers with large cubic pores at all corners. The surfactant (CPC) plays a key role for the truncation of cube corners, which initialize the ultimate pore opening sites, and the subsequent formation of cross-belt walls with square pores specially confined at the corner sites. This study suggests that the morphology of hollow particles can be controlled in the presence of specific surfactants through room-temperature galvanic replacements, thus enabling additional tunability of their optical properties. It also advances our understanding of nanoscale galvanic replacement in the presence of surface-capping agents, which can be extended to a wide range of materials and reactions. Furthermore, by exploiting the conformational responsiveness of particle coronas, we demonstrate the potential of nanowrappers as nanoparticle carriers, and their use for targeted release of nanoparticles. This work offers a promising strategy for designing and constructing multifunctional architectures based on porous hollow nanostructures.

ASSOCIATED CONTENT

Supporting Information

The Supporting Information is available free of charge on the ACS Publications website at DOI: 10.1021/acscentsci.8b00778.

Additional experimental details and figures including TEM images, 3D rendering images, SEM images, optical extinction spectra, numerical simulations of optical spectra, and DLS analyses (PDF)

Movie S1: animated view of the 3D morphology tomographic reconstruction of nanowrapper (MPG)

AUTHOR INFORMATION

Corresponding Author

*E-mail: flu@bnl.gov.

ORCID

Fang Lu: 0000-0003-3765-7615

Mingzhao Liu: 0000-0002-0999-5214

Weiping Cai: 0000-0002-4515-6098

Present Address

[○]H.X.: Department of Physics & Astronomy, University of California, Irvine, Irvine, CA 92697, USA.

Author Contributions

[▽]F.L. and H.X. contributed equally.

Notes

The authors declare no competing financial interest.

Safety statement: no unexpected or unusually high safety hazards were encountered.

ACKNOWLEDGMENTS

We thank Dr. Kevin G. Yager for useful discussion. The research was carried out at the Center for Functional Nanomaterials of Brookhaven National Laboratory, supported by the U.S. Department of Energy, Office of Basic Energy Sciences, under Contract DE-SC0012704. This work was also supported by the Natural Science Foundation of China (Grants 51531006 and 11574313).

REFERENCES

(1) Genc, A.; Patarroyo, J.; Sancho-Parramon, J.; Bastus, N. G.; Puntes, V.; Arbiol, J. Hollow metal nanostructures for enhanced plasmonics: synthesis, local plasmonic properties and applications. *Nanophotonics* **2017**, *6* (1), 193−213.

(2) Fang, Z. C.; Wang, Y. C.; Liu, C. X.; Chen, S.; Sang, W.; Wang, C.; Zeng, J. Rational Design of Metal Nanoframes for Catalysis and Plasmonics. *Small* **2015**, *11* (22), 2593−2605.

(3) Mahmoud, M. A.; O'Neil, D.; El-Sayed, M. A. Hollow and Solid Metallic Nanoparticles in Sensing and in Nanocatalysis. *Chem. Mater.* **2014**, *26* (1), 44−58.

(4) Xia, Y. N.; Li, W. Y.; Cobley, C. M.; Chen, J. Y.; Xia, X. H.; Zhang, Q.; Yang, M. X.; Cho, E. C.; Brown, P. K. Gold Nanocages: From Synthesis to Theranostic Applications. *Acc. Chem. Res.* **2011**, *44* (10), 914−924.

(5) Zhang, W. Q.; Rahmani, M.; Niu, W. X.; Ravaine, S.; Hong, M. H.; Lu, X. M. Tuning Interior Nanogaps of Double-shelled Au/Ag Nanoboxes for Surface-Enhanced Raman Scattering. *Sci. Rep.* **2015**, *5*, 8382.

(6) Gonzalez, E.; Arbiol, J.; Puntes, V. F. Carving at the Nanoscale: Sequential Galvanic Exchange and Kirkendall Growth at Room Temperature. *Science* **2011**, *334* (6061), 1377−1380.

(7) Chen, J. Y.; McLellan, J. M.; Siekkinen, A.; Xiong, Y. J.; Li, Z. Y.; Xia, Y. N. Facile synthesis of gold-silver nanocages with controllable pores on the surface. *J. Am. Chem. Soc.* **2006**, *128* (46), 14776−14777.

(8) Chen, C.; Kang, Y. J.; Huo, Z. Y.; Zhu, Z. W.; Huang, W. Y.; Xin, H. L. L.; Snyder, J. D.; Li, D. G.; Herron, J. A.; Mavrikakis, M.; et al. Highly Crystalline Multimetallic Nanoframes with Three-Dimensional Electrocatalytic Surfaces. *Science* **2014**, *343* (6177), 1339−1343.

(9) Lu, X. M.; Au, L.; McLellan, J.; Li, Z. Y.; Marquez, M.; Xia, Y. N. Fabrication of cubic nanocages and nanoframes by dealloying Au/Ag alloy nanoboxes with an aqueous etchant based on Fe(NO3)(3) or NH4OH. *Nano Lett.* **2007**, *7* (6), 1764−1769.

(10) Yang, M.; Chan, H.; Zhao, G. P.; Bahng, J. H.; Zhang, P. J.; Kral, P.; Kotov, N. A. Self-assembly of nanoparticles into biomimetic capsid-like nanoshells. *Nat. Chem.* **2017**, *9* (3), 287−294.

(11) Peng, P.; Lin, X. M.; Liu, Y. Z.; Filatov, A. S.; Li, D. G.; Stamenkovic, V. R.; Yang, D. L.; Prakapenka, V. B.; Lei, A. W.; Shevchenko, E. V. Binary Transition-Metal Oxide Hollow Nanoparticles for Oxygen Evolution Reaction. *ACS Appl. Mater. Interfaces* **2018**, *10* (29), 24715−24724.

(12) Xia, X. H.; Wang, Y.; Ruditskiy, A.; Xia, Y. N. 25th Anniversary Article: Galvanic Replacement: A Simple and Versatile Route to Hollow Nanostructures with Tunable and Well-Controlled Properties. *Adv. Mater.* **2013**, *25* (44), 6313−6333.

(13) Tian, L. M.; Gandra, N.; Singamaneni, S. Monitoring Controlled Release of Payload from Gold Nanocages Using Surface Enhanced Raman Scattering. *ACS Nano* **2013**, *7* (5), 4252−4260.

(14) Shevchenko, E. V.; Bodnarchuk, M. I.; Kovalenko, M. V.; Talapin, D. V.; Smith, R. K.; Aloni, S.; Heiss, W.; Alivisatos, A. P. Gold/Iron Oxide Core/Hollow-Shell Nanoparticles. *Adv. Mater.* **2008**, *20* (22), 4323−4329.

(15) El-Toni, A. M.; Habila, M. A.; Labis, J. P.; Alothman, Z. A.; Alhoshan, M.; Elzatahry, A. A.; Zhang, F. Design, synthesis and applications of core-shell, hollow core, and nanorattle multifunctional nanostructures. *Nanoscale* **2016**, *8* (5), 2510−2531.

(16) Jaiswal, A.; Tian, L. M.; Tadepalli, S.; Liu, K. K.; Fei, M.; Farrell, M. E.; Pellegrino, P. M.; Singamaneni, S. Plasmonic Nanorattles with Intrinsic Electromagnetic Hot-Spots for Surface Enhanced Raman Scattering. *Small* **2014**, *10* (21), 4287−4292.

(17) Polavarapu, L.; Zanaga, D.; Altantzis, T.; Rodal-Cedeira, S.; Pastoriza-Santos, I.; Perez-Juste, J.; Bals, S.; Liz-Marzan, L. M. Galvanic Replacement Coupled to Seeded Growth as a Route for Shape-Controlled Synthesis of Plasmonic Nanorattles. *J. Am. Chem. Soc.* **2016**, *138* (36), 11453−11456.

DOI: 10.1021/acscentsci.8b00778
ACS Cent. Sci. 2018, 4, 1742−1750

(18) Liu, J.; Qiao, S. Z.; Chen, J. S.; Lou, X. W.; Xing, X. R.; Lu, G. Q. Yolk/shell nanoparticles: new platforms for nanoreactors, drug delivery and lithium-ion batteries. *Chem. Commun.* **2011**, *47* (47), 12578−12591.
(19) Stuart, M. A. C.; Huck, W. T. S.; Genzer, J.; Muller, M.; Ober, C.; Stamm, M.; Sukhorukov, G. B.; Szleifer, I.; Tsukruk, V. V.; Urban, M.; et al. Emerging applications of stimuli-responsive polymer materials. *Nat. Mater.* **2010**, *9* (2), 101−113.
(20) Kuroki, H.; Tokarev, I.; Nykypanchuk, D.; Zhulina, E.; Minko, S. Stimuli-Responsive Materials with Self-Healing Antifouling Surface via 3D Polymer Grafting. *Adv. Funct. Mater.* **2013**, *23* (36), 4593−4600.
(21) Zhang, Y. G.; Pal, S.; Srinivasan, B.; Vo, T.; Kumar, S.; Gang, O. Selective transformations between nanoparticle superlattices via the reprogramming of DNA-mediated interactions. *Nat. Mater.* **2015**, *14* (8), 840−847.
(22) Zhan, P. F.; Dutta, P. K.; Wang, P. F.; Song, G.; Dai, M. J.; Zhao, S. X.; Wang, Z. G.; Yin, P.; Zhang, W.; Ding, B. Q.; et al. Reconfigurable Three-Dimensional Gold Nanorod Plasmonic Nanostructures Organized on DNA Origami Tripod. *ACS Nano* **2017**, *11* (2), 1172−1179.
(23) Sun, Y. G.; Xia, Y. N. Mechanistic study on the replacement reaction between silver nanostructures and chloroauric acid in aqueous medium. *J. Am. Chem. Soc.* **2004**, *126* (12), 3892−3901.
(24) Yavuz, M. S.; Cheng, Y. Y.; Chen, J. Y.; Cobley, C. M.; Zhang, Q.; Rycenga, M.; Xie, J. W.; Kim, C.; Song, K. H.; Schwartz, A. G.; et al. Gold nanocages covered by smart polymers for controlled release with near-infrared light. *Nat. Mater.* **2009**, *8* (12), 935−939.
(25) Au, L.; Chen, Y. C.; Zhou, F.; Camargo, P. H. C.; Lim, B.; Li, Z. Y.; Ginger, D. S.; Xia, Y. N. Synthesis and Optical Properties of Cubic Gold Nanoframes. *Nano Res.* **2008**, *1* (6), 441−449.
(26) Sun, X. J.; Kim, J.; Gilroy, K. D.; Liu, J. Y.; Konig, T. A. F.; Qin, D. Gold-Based Cubic Nanoboxes with Well-Defined Openings at the Corners and Ultrathin Walls Less Than Two Nanometers Thick. *ACS Nano* **2016**, *10* (8), 8019−8025.
(27) Niu, W. X.; Zheng, S. L.; Wang, D. W.; Liu, X. Q.; Li, H. J.; Han, S. A.; Chen, J.; Tang, Z. Y.; Xu, G. B. Selective Synthesis of Single-Crystalline Rhombic Dodecahedral, Octahedral, and Cubic Gold Nanocrystals. *J. Am. Chem. Soc.* **2009**, *131* (2), 697−703.
(28) Lu, F.; Zhang, Y.; Liu, S. Z.; Lu, D. Y.; Su, D.; Liu, M. Z.; Zhang, Y. G.; Liu, P.; Wang, J. X.; Adzic, R. R.; et al. Surface Proton Transfer Promotes Four-Electron Oxygen Reduction on Gold Nanocrystal Surfaces in Alkaline Solution. *J. Am. Chem. Soc.* **2017**, *139* (21), 7310−7317.
(29) Hamon, C.; Postic, M.; Mazari, E.; Bizien, T.; Dupuis, C.; Even-Hernandez, P.; Jimenez, A.; Courbin, L.; Gosse, C.; Artzner, F.; et al. Three-Dimensional Self-Assembling of Gold Nanorods with Controlled Macroscopic Shape and Local Smectic B Order. *ACS Nano* **2012**, *6* (5), 4137−4146.
(30) Tao, A. R.; Ceperley, D. P.; Sinsermsuksakul, P.; Neureuther, A. R.; Yang, P. D. Self-Organized Silver Nanoparticles for Three-Dimensional Plasmonic Crystals. *Nano Lett.* **2008**, *8* (11), 4033−4038.
(31) Henzie, J.; Grunwald, M.; Widmer-Cooper, A.; Geissler, P. L.; Yang, P. D. Self-assembly of uniform polyhedral silver nanocrystals into densest packings and exotic superlattices. *Nat. Mater.* **2012**, *11* (2), 131−137.
(32) Lu, F.; Tian, Y.; Liu, M.; Su, D.; Zhang, H.; Govorov, A. O.; Gang, O. Discrete Nanocubes as Plasmonic Reporters of Molecular Chirality. *Nano Lett.* **2013**, *13* (7), 3145−3151.
(33) Moreau, L. M.; Schurman, C. A.; Kewalramani, S.; Shahjamali, M. M.; Mirkin, C. A.; Bedzyk, M. J. How Ag Nanospheres Are Transformed into AgAu Nanocages. *J. Am. Chem. Soc.* **2017**, *139* (35), 12291−12298.
(34) Gomez-Grana, S.; Goris, B.; Altantzis, T.; Fernandez-Lopez, C.; Carbo-Argibay, E.; Guerrero-Martinez, A.; Almora-Barrios, N.; Lopez, N.; Pastoriza-Santos, I.; Perez-Juste, J.; et al. Au@Ag Nanoparticles: Halides Stabilize {100} Facets. *J. Phys. Chem. Lett.* **2013**, *4* (13), 2209−2216.
(35) Ghosh, S.; Manna, L. The Many "Facets" of Halide Ions in the Chemistry of Colloidal Inorganic Nanocrystals. *Chem. Rev.* **2018**, *118* (16), 7804−7864.
(36) Xiong, H. M.; Sfeir, M. Y.; Gang, O. Assembly, Structure and Optical Response of Three-Dimensional Dynamically Tunable Multicomponent Superlattices. *Nano Lett.* **2010**, *10* (11), 4456−4462.
(37) Hamon, C.; Martini, C.; Even-Hernandez, P.; Boichard, B.; Voisin, H.; Largeau, L.; Gosse, C.; Coradin, T.; Aime, C.; Marchi, V. An aqueous one-pot route to gold/quantum rod heterostructured nanoparticles functionalized with DNA. *Chem. Commun.* **2015**, *51* (89), 16119−16122.
(38) Maye, M. M.; Nykypanchuk, D.; van der Lelie, D.; Gang, O. A simple method for kinetic control of DNA-induced nanoparticle assembly. *J. Am. Chem. Soc.* **2006**, *128* (43), 14020−14021.

DOI: 10.1021/acscentsci.8b00778
ACS Cent. Sci. 2018, 4, 1742−1750